Conf-9411144--160

UCRL-JC-119216
PREPRINT

Magnetic X-Ray Circular Dichroism in Nickel-Gold Multilayers

A. F. Jankowski
G. D. Waddill
J. G. Tobin

This paper was prepared for submittal to the
Fall Meeting of the Materials Research Society
Boston, Massachusetts
November 28–December 2, 1994

November 11, 1994

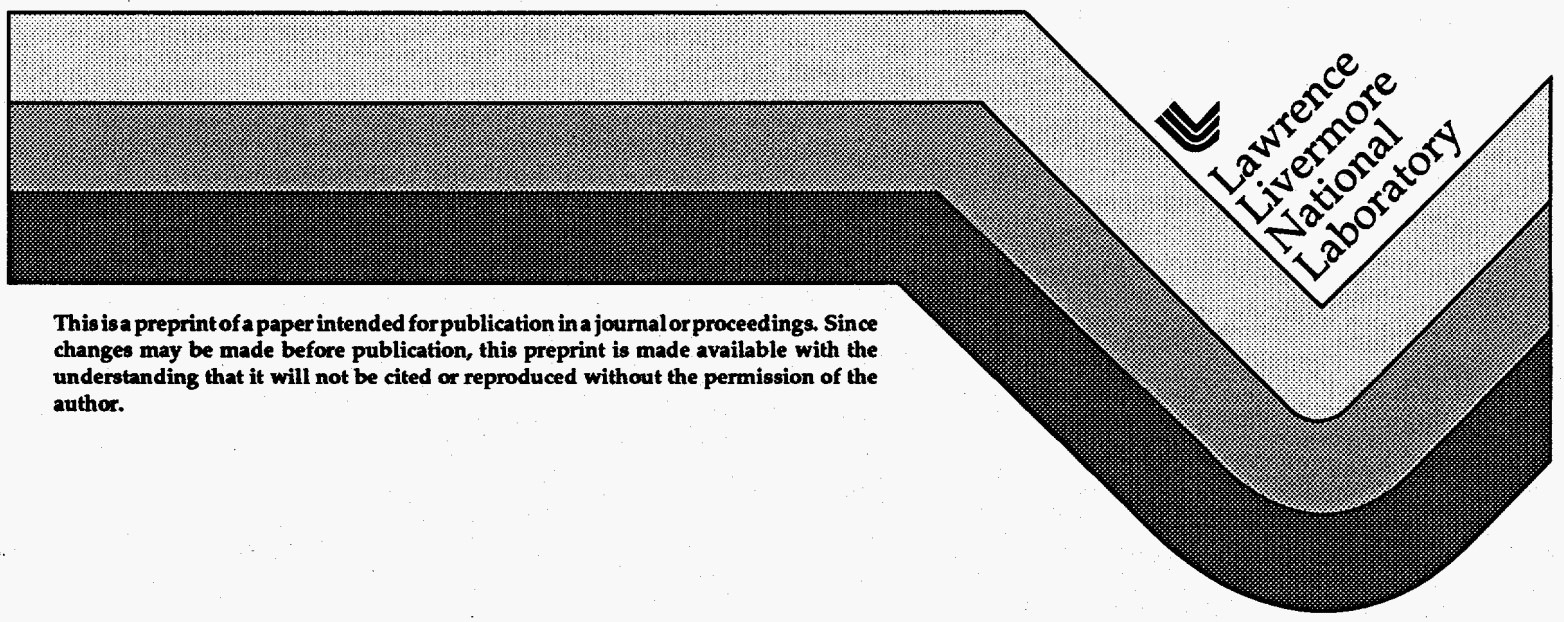

DISCLAIMER

Portions of this document may be illegible in electronic image products. Images are produced from the best available original document.

MAGNETIC X-RAY CIRCULAR DICHROISM IN NICKEL-GOLD MULTILAYERS

A.F. JANKOWSKI*, G.D. WADDILL**, and J.G. TOBIN*
*Lawrence Livermore National Laboratory, Livermore, CA 94551-9900 U.S.A.
**University of Missouri, Physics Department, Rolla, MO 65401-0249 U.S.A.

ABSTRACT

Magnetic circular dichroism in x-ray absorption is used to investigate the in-plane, remnant magnetization of well-characterized $Ni_{0.48}/Au_{0.52}$ multilayers. Large superlattice strains are found in this multilayer system for samples with a 2nm layer pair spacing. A larger dichroism is found in the Ni 2p absorption edge for a 1.8nm than for a 4.4nm layer pair sample. The larger dichroism is consistent with a larger magnitude of in-plane strain for the Ni layers and a larger total magnetic anisotropy energy as previously shown from magnetization curves.

INTRODUCTION

The observation of magnetic anisotropy in the metallic multilayer systems proves to be of interest for magnetic recording and magneto-optic applications. In general, the magnetic properties of metallic multilayer films are strongly dependent on the relative as well as absolute layer thicknesses. Conventional magnetometry is typically used to investigate magnetization and anisotropy of metallic films. Beyond this application, x-ray absorption spectroscopy (XAS) can be used for measuring magnetic circular dichroism (MCD) - providing a sensitive technique for monitoring elemental specific changes in the orientation of sample magnetization.[1] For example, the remnant magnetization of Fe and Co are measured as a function of layer thickness for a series of Fe_xCo_{1-x}/Pt multilayer thin films using MCD.[2-4]

The microstructure of Ni/Au multilayer samples prepared by sputter deposition have been characterized using high resolution electron microscopy, selected area diffraction and x-ray diffraction.[5-8] A net expansion of the superlattice is measured along the growth direction for 2 $\pm$ 0.5 nm layer pair spacings. In addition, a coherent-to-incoherent (in-plane) transition at the layer interfaces was found for samples with repeat spacings greater than 2 nm. Enhanced physical properties have been linked to this characteristic structural feature as, for example, a two-fold increase in microhardness.[9]

The magnetic properties of the $Ni_{0.48}/Au_{0.52}$ multilayers have been studied as a function of the Ni layer thickness using vibrating sample magnetometry and a superconducting quantum interference device.[10] It was found that the saturation magnetization (M_s) of Ni decreased inversely with the Ni layer thickness (d_{Ni}) while the Curie temperature (T_c) followed a power law

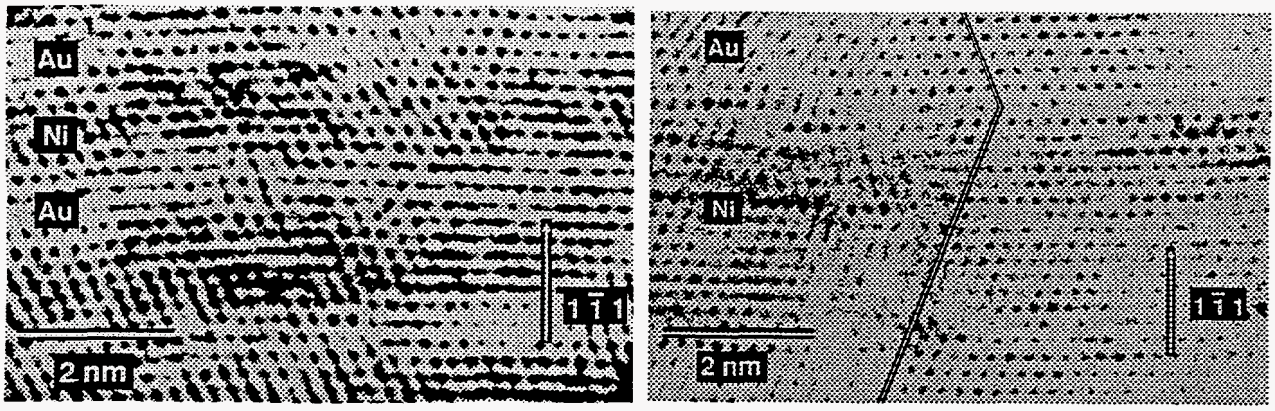

Figure 1 - High resolution lattice imaging of the (a) 1.8nm layer pair (left) and (b) 4.4nm layer pair (right) Ni/Au superlattices as viewed in cross-section.[6]

behavior. Unlike these dependencies on layer thickness, an abrupt decrease in the magnetic anisotropy is found for layer pair spacings beyond the coherent-to-incoherent transition. In this study, MCD is used to further investigate the spin and orbital components of magnetic anisotropy for two Ni/Au samples which characterize the extremes in the magnitude of superlattice strain.

MULTILAYER PREPARATION & CHARACTERIZATION

The Ni/Au multilayer samples are prepared using sputter deposition.[6,9,11] The deposition chamber is cryogenically pumped to a base pressure of 6.7×10^{-6} Pa. A circular array of planar magnetron sources is situated 20 cm beneath an oxygen-free copper platen. The purity of the target materials is 0.99995 Ni and >0.9994 Au. The magnetron sources are operated in the dc mode using an argon working gas pressure of 0.67 Pa at a flow rate of 20 cc min^{-1}. The Si(111) substrates are sequentially rotated over each source and remain at a temperature between 293 and 306 K during the deposition. The sputter deposition rates of 0.10 to 1.0 nm sec^{-1} are monitored using calibrated quartz crystals. The layer pair thickness ($d_{Ni/Au}$) and number of layer pairs (N) are indicated in Table I. X-ray diffraction was used to verify the layer pair thickness.[5-8]

Structural studies of the Ni/Au multilayers have been performed using transmission electron microscopy. The films are found to be dense columnar deposits with a (111) textured growth and random in-plane orientation.[6,11] High resolution imaging is used to reveal the multilayer lattice structure. Lattice images in cross-section are recorded at the Scherzer defocus condition using a 400 keV electron beam. The Ni/Au multilayer samples are strained layered superlattices (Figs. 1a,b).[6] Defects in the superlattice are characterized by dislocations in the Ni layers along [-111]. The lattice misfit between the Au and Ni layers is accomodated almost entirely by dislocations within the Ni layers for the 4.4nm repeat periodicity. For the region of the 4.4nm Ni/Au sample shown, misfit dislocations along [-111] accomodate 12.5% of the 13.6% Ni-Au misfit. (For the nearly incoherent superlattices, as the 4.4nm layer pair sample, the Au layers

form twin boundaries on the Ni layers - which also contain in-plane [1-10] dislocations.) However, for the 1.8nm sample, all but a few (3.2) percent of the Ni-Au misfit is accomodated by in-plane strain as divided between the Ni layer (in tension) and Au layer (in compression). Selected area diffraction patterns of individual columns (in cross-section) are used to compute the in-plane lattice spacings of the Ni layers, hence the coherency lattice strains $\varepsilon_{[2\text{-}20]}$, as well as the lattice strain along the growth direction $\varepsilon_{[111]}$.[6] Note that these strain values indicate a non-Poisson behavior indicating expansion both in-plane and along the growth direction. The strain values (listed in Table I) are comparable with the present results from the dislocation-strain analysis for the lattice images of Figs. 1a,b.

Table I. Ni/Au Multilayer Parameters

$d_{Ni/Au}$	N	$\varepsilon_{[2\text{-}20]}$	$\varepsilon_{[111]}$	μ_{SR}^{L}	μ_{SR}^{S}	μ_{SR}	μ_{BR}	K_u
1.8	193	0.059	0.078	0.068	0.182	0.250	0.165	3.25
4.4	100	0.014	0.020	0.033	0.016	0.049	0.000	1.70

MCD MEASUREMENT & ANALYSIS

The x-ray absorption spectroscopy (XAS) and magnetic circular dichroism (MCD) measurements (Figs. 2a,b) are performed on a spherical grating monochromator with the ability to generate soft (80-1100 eV) x-rays with a high degree of linear or circular polarization.[12,13] The Ni/Au samples are magnetized in-situ with a pulse coil capable of generating a 3 kOe field. To observe an MCD effect, the in-plane magnetization of the Ni/Au films requires a grazing incidence geometry with alignment of the magnetization and x-ray Poynting vectors. MCD in x-ray absorption is observed as a circular polarization dependent intensity variation in the L_{III} and L_{II} edges for 3d transition metals. The x-ray absorption spectra are taken in a total (electron) yield mode by isolating the sample and measuring the neutralization current. The polarization dependence requires that the incident x-ray helicity (either parallel or anti-parallel to the direction of propagation) be aligned or anti-aligned with the sample magnetization.[1,14] MCD measures the difference in absorption between these polarized radiation conditions as the photon energy is swept through an absorption edge. The intensity difference for the L_{III} and L_{II} white lines between the parallel and anti-parallel states provides a measure of the magnetic moment as well as its orbital and spin components.

The lattice is coupled to the electron spin angular momentum through the spin-orbit interaction. Allowed transitions are determined by the dipole selection rules. In particular, we probe the 2p and 3d transitions. The relative strengths of the L_{III} and L_{II} absorption edges

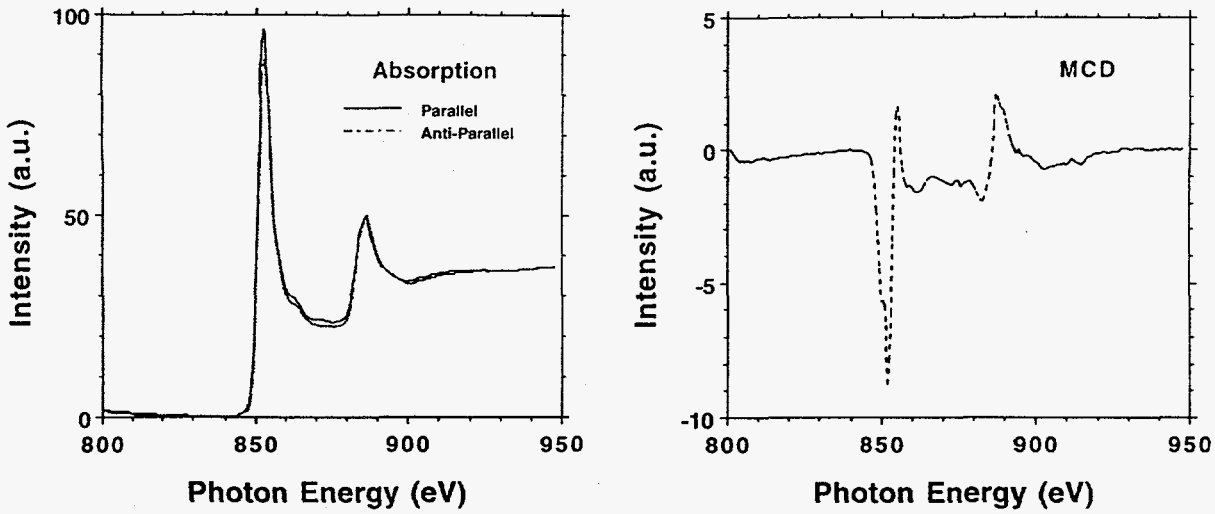

Figure 2 - The measured intensity as a function of photon energy for the (a) XAS (left) and (b) MCD (right) curves of the 1.8nm Ni/Au superlattice. The MCD curve represents the difference divided by the sum of the XAS curves.

contain information about the spin-dependent density of states near the Fermi level and the spin-orbit splitting in the d-bands (Fig. 3). Therefore, element and shell specific information is available about the spin and orbital contributions to the magnetic moments of the material.[1,15-18] Application of the sum-rule (SR) analysis yields values for the spin (μ_{SR}^{S}) and orbital (μ_{SR}^{L}) components of the total moment ($\mu_{SR} = \mu_{SR}^{S} + \mu_{SR}^{L}$). The branching-ratio (BR) analysis yields a value for the spin moment (μ_{BR}) with the apriori assumption of a small orbital moment. For 3d elements, the μ_{BR} is computed with the following relationships.[19]

$$\mu_{BR} = \text{constant} \bullet (BR^{+} - BR^{-}) \bullet (BR^{+} + BR^{-})^{-1} \quad (1)$$

$$BR^{+} = (A^{+}) \bullet (A^{+} + B^{+})^{-1} \quad (2)$$

$$BR^{-} = (A^{-}) \bullet (A^{-} + B^{-})^{-1} \quad (3)$$

where $A^{+,-}$ is the integrated intensity of the L_{III} peak above the background intensity and $B^{+,-}$ is the integrated intensity of the L_{II} peak above the background intensity for the parallel (+) and anti-parallel (-) helicity and magnetization conditions, respectively (Fig. 4). For the computation of μ_{SR}, the following equations apply.[19]

$$\mu_{SR}^{S} \cong \{\text{constant} \bullet [(A^{+}/C^{+}) - (A^{-}/C^{-})] \bullet (SUM)^{-1}\} - 3 \bullet \mu_{SR}^{L} \quad (4)$$

$$\mu_{SR}^{L} = \text{constant} \bullet [(A^{+}/C^{+}) - (A^{-}/C^{-}) + (B^{+}/C^{+}) - (B^{-}/C^{-})] \bullet (SUM)^{-1} \quad (5)$$

$$SUM = [(A^{+}/C^{+}) + (A^{-}/C^{-}) + (B^{+}/C^{+}) + (B^{-}/C^{-})] \quad (6)$$

where $C^{+,-}$ is the height of the background curves above the baseline intensity. These analysis procedures applied to the XAS and MCD spectra (Figs. 2a,b) produce values for the magnetic

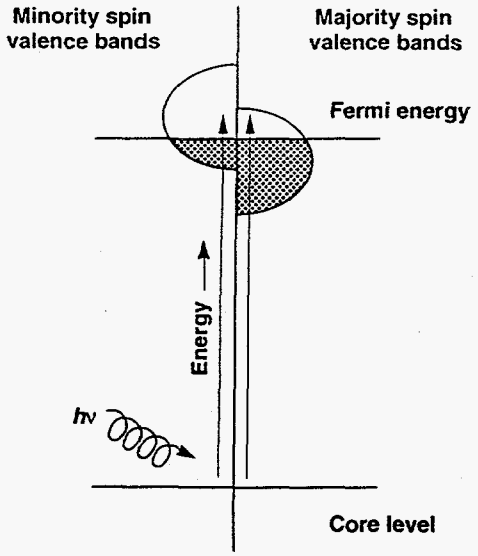

Figure 3 - A schematic (above) of the absorption of a photon and transition of an electron into an exchange split valence band density of states.

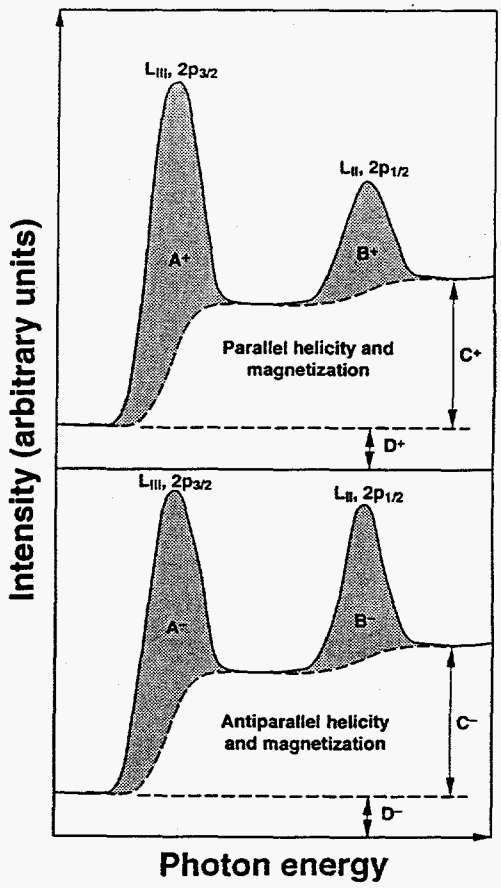

Figure 4 - A schematic (right) of x-ray absorption spectra with white line peaks at the L_{III} and L_{II} edges for the case of ferromagnetic alignment.

moments listed in Table I (in units of μ_B/Ni atom). The analyses may be complicated, however, by the polycrystalline surface. If the sample is not of a single domain, then MCD will average the domains yielding a moment that reflects the average projection of magnetization along the photon propagation direction.

DISCUSSION & SUMMARY

The total anisotropy energy K_u represents the difference in energy density between the parallel and perpendicular magnetized states. It is equivalent to the difference in area under the magnetization (versus applied field) curves. The total anisotropy energy can be expressed as

$$K_u = -\{2\pi \cdot M_s^2 + K_v + 2 \cdot K_s \cdot d_{Ni}^{-1}\} \qquad (7)$$

where K_v and K_s are the volume and surface anisotropy constants, respectively.[10] The preferred in-plane magnetization for these Ni/Au multilayers means that K_u is always negative. Representative values of K_u (10^6 erg cc^{-1}) for the samples examined with XAS for MCD are listed in Table I. Whereas the coherent-to-incoherent transition for increasing layer pair spacing was observed not to have any noticeable effect on either M_s or T_c, a lattice strain effect is apparent on K_u.

The magnetic behavior of lattice strained and unstrained Ni/Au multilayers have been probed using MCD. The MCD results are consistent with the magnetic anisotropy measurement of these films as previously determined through magnetization curves.[5] A large decrease in the spin component, from 0.182 to 0.016 μ_B/Ni atom, is found with the sum-rule analysis as the in-plane strain of the Ni layer decreases from 5.9% to 1.4% (with an increase in the Ni layer thickness from 0.91 to 2.1 nm). Results for the branching ratio analysis yield nearly equivalent results as for the spin component. The magnitude of decrease (by a factor of 2) in the total anisotropy energy K_u is equal to the decrease in the orbital component, from 0.068 to 0.033 μ_B/Ni atom, which therefore serves as an indicator of elastic strain effects on crystalline lattice. These results confirm a magneto-elastic effect in the magnetization behavior of the Ni/Au multilayer system.

ACKNOWLEDGMENTS

This work was performed under the auspices of the United States Department of Energy by Lawrence Livermore National Laboratory under contract W-7405-Eng-48.

REFERENCES

1. J.G. Tobin, G.D. Waddill and D.P. Pappas, Phys. Rev. Lett. **68**, 3642 (1992).
2. A. Jankowski, G.D. Waddill and J. Tobin, Mat. Res. Soc. Symp. Proc. **313**, 227 (1993).
3. A.F. Jankowski, G.D. Waddill and J.G. Tobin, J. Vac. Sci. Technol. A **12**, 2215 (1994).
4. J. Tobin, A. Jankowski, G. Waddill and P. Sterne, Mat. Res. Soc. Symp. Proc. **343** (1994).
5. A.F. Jankowski, Superlatt. Microstruc. **6**, 427 (1989).
6. A.F. Jankowski, J. Appl. Phys. **71**, 1782 (1992).
7. J. Chaudhuri, S. Shah, V. Gondhalekar and A. Jankowski, J. Appl. Phys. **71**, 3816 (1992).
8. J. Chaudhuri, S. Alyan and A. Jankowski, Thin Solid Films **219**, 63 (1992).
9. A.F. Jankowski, J. Magn. Magn. Mat. **126**, 185 (1993).
10. J.R. Childress, C.L. Chien and A.F. Jankowski, Phys. Rev. B **45**, 2855 (1992).
11. M.A. Wall and A.F. Jankowski, Thin Solid Films **181**, 313 (1989).
12. K.G. Tirsell and V. Karpenko, Nucl. Instrum. Meth. A **291**, 511 (1990).
13. L.J. Terminello, G.D. Waddill and J.G. Tobin, Nucl. Instrum. Meth. A **319**, 271 (1992).
14. J.L. Erskine and E.A. Stern, Phys. Rev. B **12**, 5016 (1975).
15. B.T. Thole and G. van der Laan, Phys. Rev. A **38**, 1943 (1988).
16. B.T. Thole and G. van der Laan, Phys. Rev. B **42**, 6670 (1990).
17. B.T. Thole, P. Carra, F. Sette and G. vander Laan, Phys. Rev. Lett. **68**, 1943 (1992).
18. P. Carra, B.T. Thole, M. Altarelli and X. Wang, Phys. Rev. Lett. **70**, 694 (1993).
19. J.G. Tobin, G.D. Waddill, A.F. Jankowski, P.A. Sterne and D.P. Pappas, (to be submitted).